agronomy

MDPI

Article

Efficient Damage Assessment of Rice Bacterial Leaf Blight Disease in Agricultural Insurance Using UAV Data

Chiharu Hongo [1,*], Shun Isono [2], Gunardi Sigit [3] and Eisaku Tamura [1]

[1] Center for Environmental Remote Sensing, Chiba University, Chiba 277-2835, Japan
[2] NHK (Japan Broadcasting Corporation), Osaka 540-8501, Japan
[3] Provincial Office of Food Crops and Horticulture of West Java Province, Bandung 40133, Indonesia; gunsigit@yahoo.com
* Correspondence: hongo@faculty.chiba-u.jp

Abstract: In Indonesia, where the agricultural insurance system has been in full operation since 2016, a new damage assessment estimation formula for rice diseases was created through integrating the current damage assessment method and unmanned aerial vehicle (UAV) multispectral remote sensing data to improve the efficiency and precision of damage assessment work performed for the payments of insurance claims. The new method can quickly and efficiently output objective assessment results. In this study, UAV images and bacterial leaf blight (BLB) rice damage assessment data were acquired during the rainy and dry seasons of 2021 and 2022 in West Java, Indonesia, where serious BLB damage occurs every year. The six-level BLB score (0, 1, 3, 5, 7, and 9) and damage intensity calculated from the score were used as the BLB damage assessment data. The relationship between normalized UAV data, normalized difference vegetation index (NDVI), and BLB score showed significant correlations at the 1% level. The analysis of damage intensities and UAV data for paddy plots in all cropping seasons showed high correlation coefficients with the normalized red band, normalized near-infrared band, and NDVI, similar to the results of the BLB score analysis. However, for paddy plots with damage intensities of 70% or higher, the biased numbering of the BLB score data may have affected the evaluation results. Therefore, we conducted an analysis using an average of 1090 survey points for each BLB score and confirmed a strong relationship, with correlation coefficients exceeding 0.9 for the normalized red band, normalized near-infrared band, and NDVI. Through comparing the time required by the current assessment method with that required by the assessment method integrating UAV data, it was demonstrated that the evaluation time was reduced by more than 60% on average. We are able to propose a new assessment method for the Indonesian government to achieve complete objective enumeration.

Keywords: food security; remote sensing; agricultural insurance; pest and diseases

Citation: Hongo, C.; Isono, S.; Sigit, G.; Tamura, E. Efficient Damage Assessment of Rice Bacterial Leaf Blight Disease in Agricultural Insurance Using UAV Data. *Agronomy* **2024**, *14*, 1328. https://doi.org/10.3390/agronomy14061328

Academic Editors: Jinling Zhao and Chuanjian Wang

Received: 31 March 2024
Revised: 6 June 2024
Accepted: 14 June 2024
Published: 19 June 2024

1. Introduction

Climate change is expected to expose humankind to various risks in the future. The Sixth Assessment Report released by the Intergovernmental Panel on Climate Change (IPCC) in August 2021 lists food security as a major threat [1]. Diseases, insects, droughts, and floods caused by extreme weather and other factors can damage crops and require considerable labor and costs to recover farmland and plant the next crop [2–4]. Farmers with insecure economic foundations are forced to leave their farms, which further threatens food security.

Serious damage is expected to occur primarily in developing countries, where a variety of policies have been proposed. In Indonesia, where rice is the primary crop [5], a farmer protection and empowerment law was enacted in 2013 [6]. As a result, an agricultural insurance system was launched in 2016, under which the government paid compensation for damage to rice paddies caused by pests, diseases, drought, and floods [7–9]. The

current damage assessment method in Indonesia involves selecting only three paddy plots from the terminal irrigation area, which includes approximately 50–300 plots, and having an assessor called a pest observer visually assess the damage to 10 rice plants on the diagonal of one paddy plot. The average damage to the entire damaged area is calculated based on the evaluation of 30 rice plants. In Indonesia, an objective evaluation method acceptable to insurance subscribers is required because the results of the visual damage evaluation method may differ between assessors [10,11]. Recently, there has been a growing expectation to build more robust and efficient methods for detecting paddy rice diseases using machine and deep learning, as automated approaches to detect leaf diseases can help farmers detect diseases with or without human intervention [12–15].

Promptness is especially important when operating insurance programs in Southeast Asia. A prolonged evaluation time can lead to further losses, such as missing the next rice-planting season. Indonesia has wet and dry seasons, and two or three rice crops per year are commonly grown in two or three cropping seasons. Damaged paddy fields must be maintained in their current state until damage assessors complete their evaluation; however, the limited number of assessors limits their ability to quickly produce damage assessment results. Therefore, we have improved the current evaluation method to construct a new damage assessment method that can efficiently and quickly evaluate damage and output objective evaluation results.

Bacterial leaf blight (BLB) is a serious disease that occurs annually in West Java, Indonesia, where this study was conducted. Although resistant rice varieties have been cultivated and chemicals are sprayed to ensure stable rice production, the occurrence of BLB damage has not ended and a policy to protect farmers through agricultural insurance has been adopted. The key to agricultural insurance is objective, prompt, and inexpensive damage assessment, and remote sensing technology is expected to be utilized for its advantages, such as wide-area information, immediacy, and objectivity [16]. Research has already been conducted in Indonesia using satellite data to estimate paddy rice production, the transplanting dates of rice crops, and to assess drought damage [17–20], and it has been reported that satellite remote sensing data can be applied even in Indonesia, where the area of a single paddy field is small. Meanwhile, remote sensing data has been acquired using satellites, aircraft, helicopters, and unmanned aerial vehicles, although satellite remote sensing data has limitations in understanding in-field variability, such as in precision agriculture [21]. Among these platforms, multirotor drones are the most promising for smart farming [22], and there is a need to develop a damage assessment method using unmanned aerial vehicle (UAV) remote sensing for assessment of disease damage.

Previous studies on crop diseases using remote sensing data have reported that the sensitivity of near-infrared and short-wavelength infrared reflectance to the degree of BLB infection is high [23] and that the difference in reflectance between healthy and BLB-infected rice plants is pronounced in the 770–860 nm and 920–1050 nm wavelength ranges [24]. UAV imagery analysis in rice paddies in Bali, Indonesia, confirmed that vegetation indices, normalized difference vegetation index (NDVI), enhanced vegetation index (EVI), and normalized difference red edge (NDRE) had a strong linear correlation with BLB damage intensity [25]. Studies using aircraft and UAV observation data have evaluated the severity of BLB, rice blast, and rice spot disease [26–28]. Studies have also reported examining crop growth monitoring using an RGB camera on a UAV, from a low-cost perspective [29,30]. Studies using satellite observation data to detect crop diseases have included the detection of rice blast, rice sesame leaf blight, and yellow rust [31,32]. Studies using multispectral data from LISS-IV satellite observations to detect rice stress caused by BLB at the regional level [33] and a study evaluating the correlation between BLB damage severity and spectral indices from Sentinel-2 data have also been reported [34–36]. These reports show that reflectance data in the visible and near-infrared regions and vegetation indices calculated from reflectance are useful for understanding BLB and other diseases.

Therefore, this study reports a precise assessment of BLB damage using UAV multispectral remote sensing data in West Java, Indonesia, where serious BLB damage occurs

annually, and examines the feasibility of reducing the damage assessment time via integrating current assessment methods and UAV data to create a new damage assessment estimation formula.

2. Materials and Methods

2.1. Study Area

The target area for this study was the Cihea Irrigation District (6°50′ S, 107°16′ E) in the northeastern part of Cihea, Cianjur Province, West Java, Republic of Indonesia (Figure 1a). This area is located just below the equator and has a tropical climate throughout the year, with a dry season from April to October and a rainy season from November to March. In this study, both dry and rainy season cropping from 2021 to 2022 were considered.

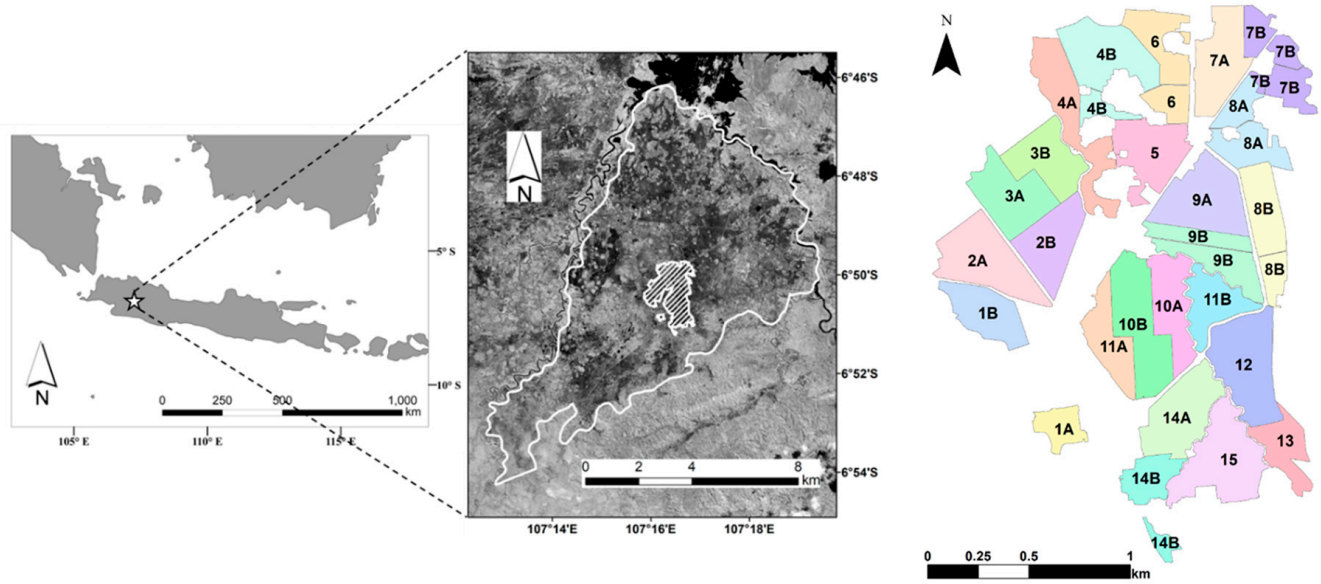

(**a**) (**b**)

Figure 1. Study area; (**a**) Cihea Irrigation District, (**b**) 250-hectare test area with irrigation block name.

The target area was a large irrigated district of approximately 8000 ha. Severe damage occurred annually over a wide area because the BLB bacteria that developed at one location were carried downstream by irrigation water and spread over the entire area. In addition, the shape and size of the fields were not uniform, and each irrigated area was characterized by a mixture of fields at different growth stages owing to different planting times. In this study, the 250 ha irrigated area shown in Figure 1b was set as a test site, and several irrigated areas where BLB had occurred were selected for investigation. The rice variety grown in both years was Inpari 32, and the soil type in the area was identified as Inceptisol based on our previous soil auger and soil cross-sectional surveys [17].

2.2. Characteristics of the Target Disease; Bacterial Leaf Blight Disease of Rice

BLB is a disease caused by Xanthomonas oryzae pv. Studies on bacteriophages have shown that bacteria are transported through the flow of irrigation water. The disease has been confirmed to occur in rice-growing regions worldwide, including tropical and temperate Asia, West Africa, and Central and South America [37,38]. Breeding disease-resistant varieties is an effective and economical method for controlling BLB [39]. Resistant varieties have been introduced to the study area in recent years; however, disease outbreaks remain uncontrolled.

The disease symptoms of BLB include yellowing at the leaf margins, yellow irregular spots, or blotches that gradually expand and merge into wavy lesions that turn yellowish white or white and then turn grayish white and die at the tip of the leaf [40]. The border

between the dead and healthy areas, that is, near the leaf margins and lesions, is marked by the appearance of small yellow granular mucilage masses that overflow from the pores and harden, distinguishing it from natural mortality. Figure 2 shows the symptoms of BLB with different degrees of damage observed in the field.

Figure 2. BLB outbreak plots (**left**: score 3, **right**: score 7).

BLB increases the risk of yield loss early in the infected growth stage. Therefore, proper cultivation and management are important. Major measures include the cultivation of resistant varieties, removal of weeds, stumps, and seedlings that harbor the fungus, and spraying with pesticides.

2.3. Current Damage Assessment Method in Agricultural Insurance in Indonesia

Damage assessments in agricultural insurance are performed by loss assessors known as pest observers, who are local state government employees. Visual assessment is conducted based on the method indicated in the guidelines for damage assessment procedures prepared by the Ministry of Agriculture of Indonesia. In recent years, the aging and understaffing of pest observers have become major problems, and the area covered by a single pest observer can be as large as 5000–9000 ha.

An outline of the current BLB damage assessment methodology is shown in Figure 3. Three rice paddy plots were placed proportionally on the diagonal within the minimum level irrigation area, and these were set as the plots to be evaluated. Then, in the three selected plots, 10 plants in each plot diagonal were visually evaluated (a total of 30 plants). The degree of BLB damage was evaluated on a six-point scale (0, 1, 3, 5, 7, and 9) for each plant according to the area of diseased leaves. A higher score number indicated more severe BLB damage. Then, the BLB damage rate was calculated using the following formula, using the BLB scores of the 30 evaluated plants:

$$\text{BLB damage intensity}(\%) = \frac{n_1 + n_2 + \cdots + n_{30}}{9 \times 30} \times 100 \quad (1)$$

where n indicates the BLB damage score of each plant using the six grades.

The BLB damage intensity calculated from Equation (1) was the damage intensity for the entire area, reflecting the BLB scores of 30 plants in total for the three selected plots in the area.

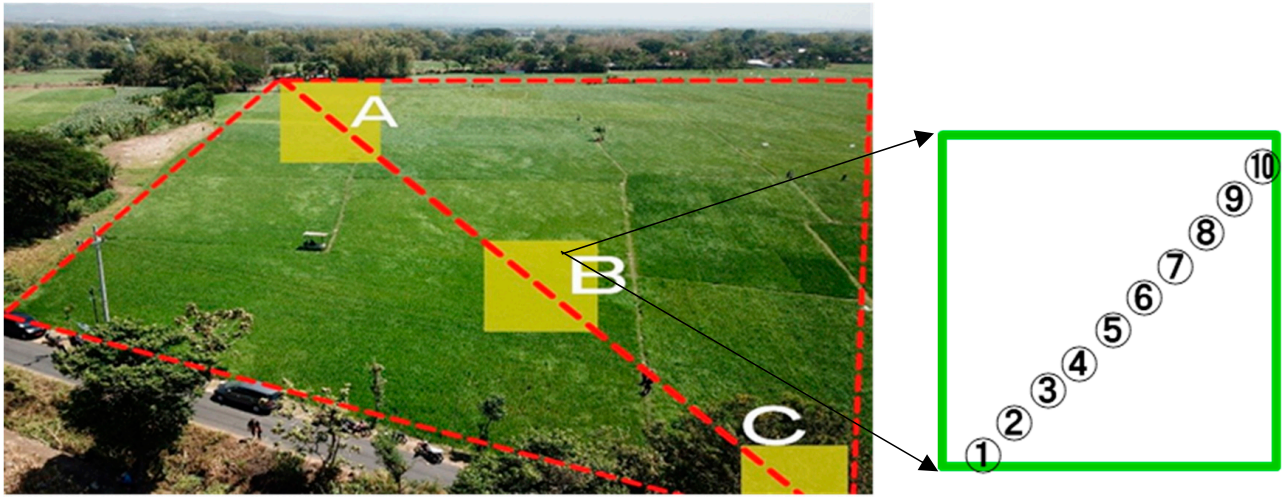

Figure 3. Outline of the current BLB damage assessment; Three paddy plots, A, B, and C, were proportionally located on the diagonal within the minimum irrigation zone and used as evaluation plots.

2.4. Field Survey Data

BLB damage scores were assessed in 109 plots: 9 plots during the wet season from 31 December 2020, to 5 March 2021; 30 plots during the dry season from 19 May to 12 August 2021; 18 plots during the transition from the dry to wet season from 12 October to 3 December 2021; 23 plots during the wet season from 1 March to 6 April 2022; and 29 plots during the dry season from July 7 to 11 September 2022. At approximately 10 d intervals during each growing season, pest observers evaluated the damage scores according to the current method, and aerial data were acquired using a UAV.

2.5. UAV Image Data

Aerial images were acquired synchronously with field survey data using a Bluegrass Fields (Parrot Inc., New York, NY, USA) device equipped with a Sequoia multispectral camera with an observation wavelength range from visible to near-infrared. A sunshine sensor module was attached to the top of the camera to calibrate the image according to the intensity of sunlight.

In addition to preliminary observations under various conditions, we used a radiative transfer model to estimate the effect of the solar radiation environment on the reflectance measurements acquired via the UAV camera. While the effect of solar altitude was not observed under cloudy conditions, where scattered light predominated, it was found that under clear skies, red reflectance increased when the solar altitude was high, and near-infrared reflectance increased when the solar altitude was low [41]. Therefore, it was found that taking images at times when the solar altitude was between 45 °and 65 °reduced the influence of the solar radiation environment; therefore, aerial images were obtained at times when the sun was at this altitude. The ground altitude and overlap ratio were determined through considering the time when UAV flights were possible, the area to be analyzed, and the resolution. The overlap–sidelap ratio was 80–90% and the altitude was 50–60 m, with a speed of 5 m/s and a ground sample distance (GDS) of 2.6–3.0 cm/pixel.

The acquisition dates of field data and UAV data used to create the estimation equation for BLB scores and the digitization footprint size of captured images are shown in Table 1.

Table 1. The data acquisition date and the digitization footprint size of captured images.

Field and UAV Data Acquisition Date	BLB Assessment Plot and Point	Digitization Footprint (Mb/ha)
25 February 2021	6, 60	2336.4
5 March 2021	3, 30	1845.6
19 July 2021	3, 30	3549.8
21 July 2021	3, 30	3106.2
22 July 2021	3, 30	3403.3
28 July 2021	1, 10	2570.0
29 July 2021	3, 30	3314.8
30 July 2021	3, 30	4015.8
7 August 2021	3, 30	3691.8
10 August 2021	3, 30	2835.5
11 August 2021	5, 50	3862.0
12 August 2021	3, 30	2857.5
22 November 2021	3, 30	3138.0
23 November 2021	6, 60	3860.1
30 November 2021	3, 30	3537.8
1 December 2021	3, 30	3299.5
2 December 2021	1, 10	3407.4
3 December 2021	2, 20	3280.1
5 March 2022	3, 30	3197.5
25 March 2022	3, 30	3356.9
28 March 2022	3, 30	2500.6
4 April 2022	6, 60	3160.7
5 April 2022	3, 30	3182.2
6 April 2022	5, 50	3393.6
16 August 2022	6, 60	3044.3
17 August 2022	3, 30	3418.4
29 August 2022	6, 60	3276.5
30 August 2022	6, 60	3447.0
31 August 2022	3, 30	3230.4
10 September 2022	2, 20	3886.7
11 September 2022	3, 30	3610.8

2.6. Creation of Orthomosaic Image

Metashape Professional version 1.8 (Agisoft) with integrated SfM-MVS (Structure from Motion and Multi-View Stereo) was used to create orthomosaic images. The software analysis procedure consisted of capturing the UAV images after shooting, reflectivity calibration, alignment adjustment, adjustment and optimization of camera parameters, high-density cloud construction, DSM creation, and orthomosaic image generation.

In addition, a geometric correction process using ground control points was applied between images to ensure that orthomosaic images from different time periods were not misaligned.

2.7. UAV Image Normalization Process

Because UAV data acquired in different years and seasons were used in this analysis, it was necessary to pay attention to the camera type, solar radiation conditions at the time of acquisition, and the altitude at which the data were collected. Normalized reflectance for ground-based and satellite data acquired with spectroradiometers can be used to reduce the differences in observation conditions, terrain effects, and atmospheric effects. The normalized reflectance was calculated taking advantage of the fact that the shape of the emission spectrum is similar to that of the ground-based spectra, while the emitted amount tends to vary depending on the observation conditions and due to using the additive average of the reflectance over all wavelength bands used. In this study, this method was applied to normalize UAV images to produce normalized reflectance images. The normalization procedure consisted of first calculating the additive averages of the four bands of reflectance from Equation (2) and then normalizing the reflectance of each band according to the additive averages. The additive mean and normalized reflectance of each band are expressed as follows:

$$r_0 = \frac{\text{Green} + \text{Red} + \text{Red edge} + \text{NIR}}{4} \quad (2)$$

$$\text{NGreen} = \frac{\text{Green}}{r_0} \quad (3)$$

$$\text{NRed} = \frac{\text{Red}}{r_0} \quad (4)$$

$$\text{NRed edge} = \frac{\text{Red edge}}{r_0} \quad (5)$$

$$\text{NNIR} = \frac{\text{NIR}}{r_0} \quad (6)$$

Comparing the correlation coefficients of the BLB scores with the UAV sample data before and after the normalization process, it was confirmed that the correlation coefficients were higher in all bands of reflectance; therefore, we decided to use the UAV images after normalization in this analysis.

2.8. Method for Identifying Survey Points and Extracting Reflectance Value on Images

To extract the reflectance from the orthomosaic images of the sites where the pest observers conducted the BLB damage assessment, the assessment sites were identified from the created orthomosaic images.

The resolution of the UAV image was 2.6–3.0 cm per pixel, which is high resolution. When the positional information acquired with a handheld GPS in the field was superimposed on this high-resolution image, it was difficult to capture the survey points accurately because of GPS positioning errors. Therefore, a red funnel, as shown in the aerial image (Figure 4), was placed at the survey site prior to the aerial photography, as shown in Figure 4. The diameter of the funnel was approximately 20 cm, the buffer radius was set to 50 cm, and the inner radius was set to 15 cm. The reflectance of the image corresponding to the donut-shaped portion with the inner diameter removed was extracted for analysis.

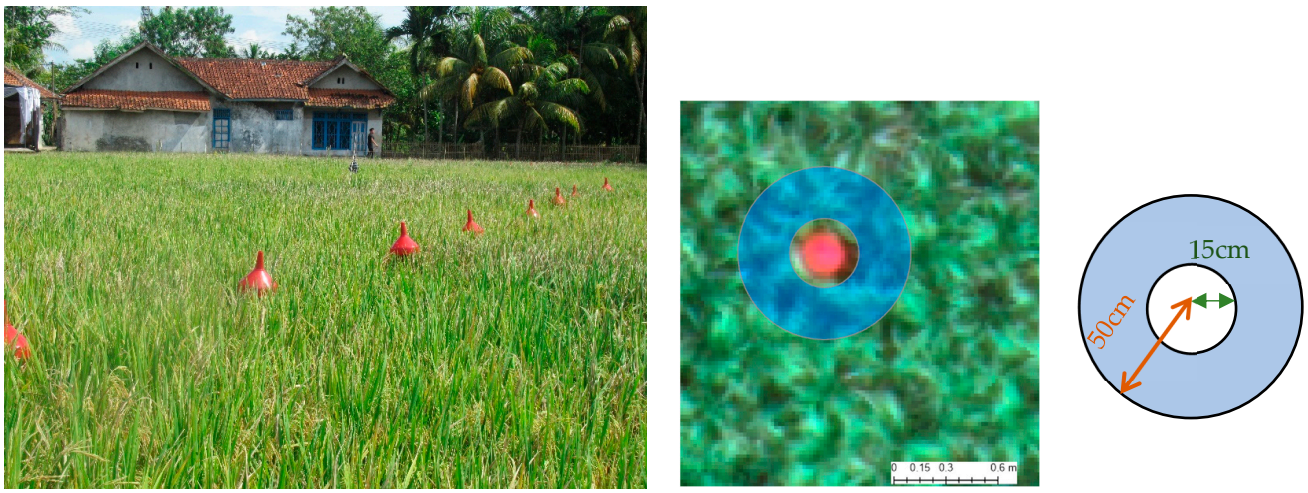

Figure 4. (**Left**) Red funnel installed at the survey site; (**Right**) red funnel on UAV image, and reflectance extraction area.

2.9. Creation of BLB Damage Assessment Estimation Equation

Multiple regression analysis was conducted using the normalized UAV green band, red band, red edge band, near-infrared band, and NDVI, GNDVI, and RGI indices as explanatory variables to develop an estimation equation for the degree of BLB damage from the averaged value calculated from 1090 survey points, followed by 5-fold cross-validation to evaluate the accuracy. Each index was calculated using the following equations:

$$\mathrm{NDVI} = (\mathrm{NIR} - \mathrm{R})/(\mathrm{NIR} + \mathrm{R})$$

$$\mathrm{GNDVI} = (\mathrm{NIR} - \mathrm{G})/(\mathrm{NIR} + \mathrm{G})$$

$$\mathrm{RGI} = \mathrm{G} \times \mathrm{Red\ Edge}$$

As described in Section 2.3, the current BLB damage assessment method, as indicated by the Indonesian Ministry of Agriculture, outputs the damage intensity for a single plot through substituting a six-level BLB score (0, 1, 3, 5, 7, and 9) for each plant unit into the formula to calculate the damage intensity. Therefore, this analysis examined the relationship between the BLB score and UAV data and between the BLB damage intensity and UAV data.

Furthermore, the effectiveness of integrating UAV data into the current BLB evaluation method was examined through comparing the time required to output the evaluation results in order to understand the efficiency of the BLB damage evaluation process.

3. Results and Discussion

3.1. Relationship between Normalized Reflectance for Each Band and Indices and BLB

We analyzed the relationship between the normalized reflectance extracted from the orthomosaic images and calculated indices and the BLB score. The BLB score was assessed based on the number of surveyed plants, with 10 plants evaluated per plot.

Figure 5 and Table 2 show the relationship between the reflectance data obtained during the dry season and the BLB score. Figure 6 and Table 3 show the relationship between the reflectance data obtained during the rainy season and the BLB score. In the dry-season data, the correlation coefficients of Nred, NNIR, and NDVI were approximately 0.5, indicating a stronger correlation than those of the other normalized reflectance data and indices. In the rainy season data, there was no significant difference in the correlation between the single-year data and the 2-year data; however, when the 2-year rainy season data were combined, it became clear whether each normalized reflectance and index had a positive or negative correlation with the BLB score (Figure 6). The relationship between the

UAV data and BLB scores for the dry and rainy seasons for all cropping seasons in 2021 and 2022 is shown in Figure 7 and Table 4. Regarding BLB disease incidence in the rainy season crops, no paddy rice with a high degree of damage, such as a score of 7 or 9, was identified, and the BLB scores of all evaluated rice were 5 or less. This is because there is more rainfall during the rainy season, which tends to wash away the rice BLB bacteria attached to the rice bodies, leaving fewer residual bacteria on the rice plants and in the field [42,43]. BLB enters rice through the water pore apertures in rice leaves and wind-driven wounds on the plant surface. Research using bacteriophages has shown that BLB can spread to other areas through irrigation [44].

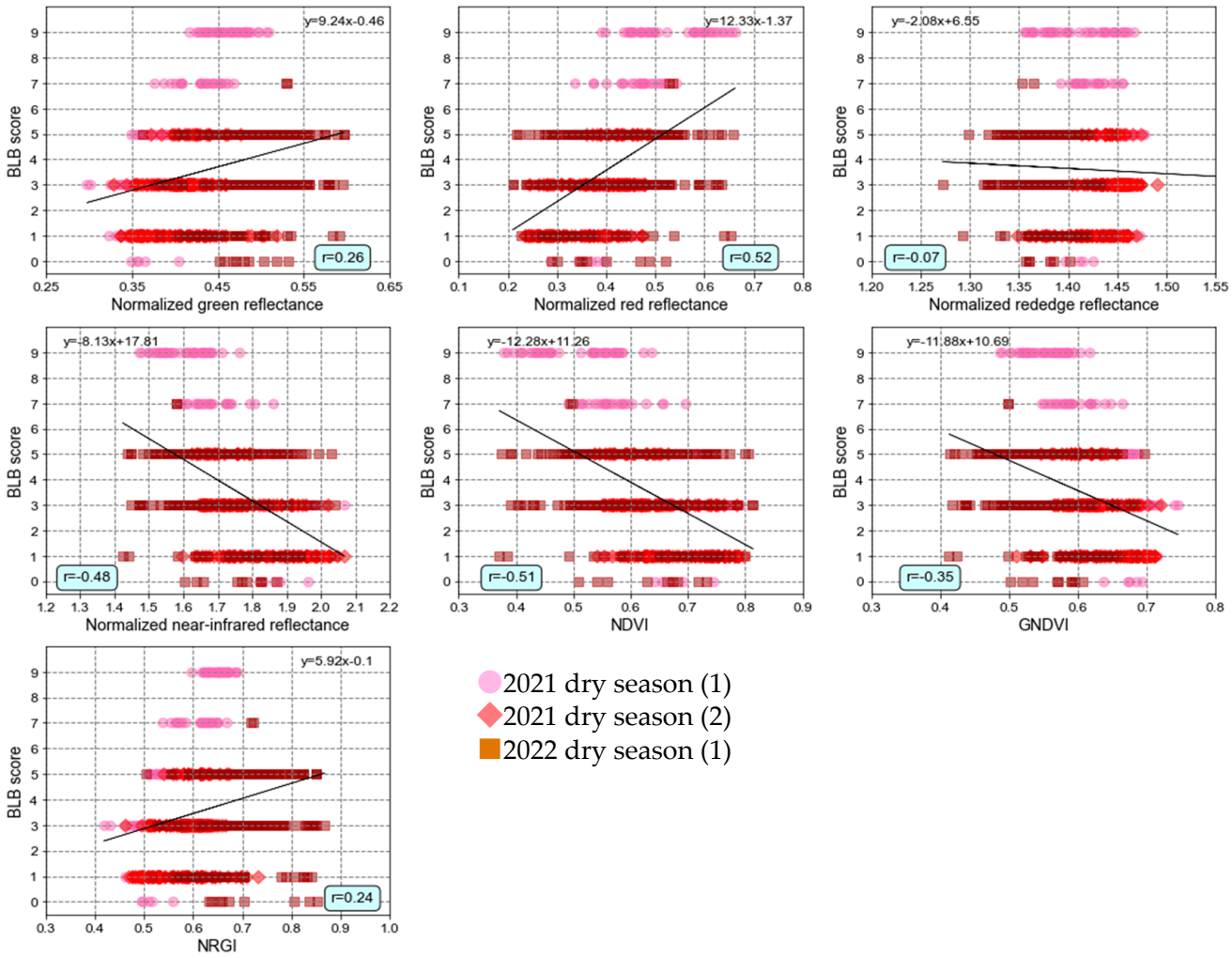

Figure 5. Relationship between UAV data and BLB scores acquired during the 2021 and 2022 dry seasons.

Table 2. Correlation coefficient between UAV data and BLB scores acquired during the 2021 and 2022 dry seasons (** significant at the 1% level).

	Ngreen	Nred	Nred Edge	NNIR	NDVI	GNDVI	NRGI
Correlation coefficient	0.261 **	0.516 **	−0.068	−0.478 **	−0.509 **	−0.354 **	0.235 **

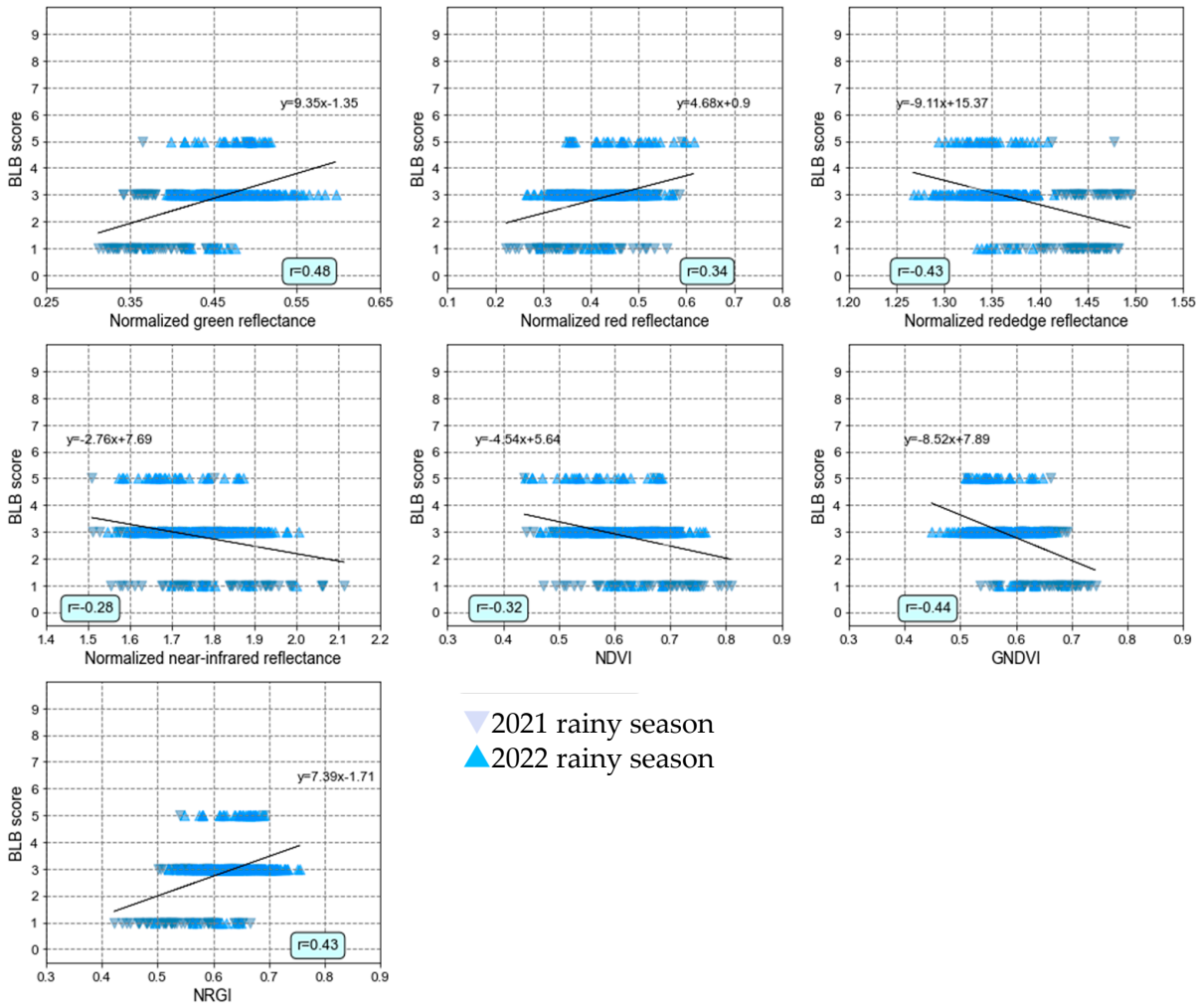

Figure 6. Relationship between UAV data and BLB scores acquired during the 2021 and 2022 rainy seasons.

Table 3. Correlation coefficient between UAV data and BLB scores acquired during the 2021 and 2022 rainy season (** significant at the 1% level).

	Ngreen	Nred	Nred Edge	NNIR	NDVI	GNDVI	NRGI
Correlation coefficient	0.481 **	0.337 **	−0.426	−0.283 **	−0.321 **	−0.443 **	0.435 **

In addition, the correlation coefficients were slightly lower than those obtained from single-year or seasonal data analyses. This was presumably due to the weighting of scores 3 and 5, because the total amount of data increased owing to the inclusion of data from all cropping seasons together, which corresponded to the increase in data with scores 3 and 5 for wet season crops. Furthermore, we observed a range of normalized reflectance and index values for the same BLB scores. One possible reason for this may be that the current assessment was based on the pest observers' visual evaluation of the BLB scores. It was necessary to be skilled in clearly separating the damage of scores 3 and 5, and it was inferred that judgment differed significantly among the evaluators. This suggests that it is necessary to incorporate UAV data into the current method and develop a damage assessment formula to obtain objective assessment results.

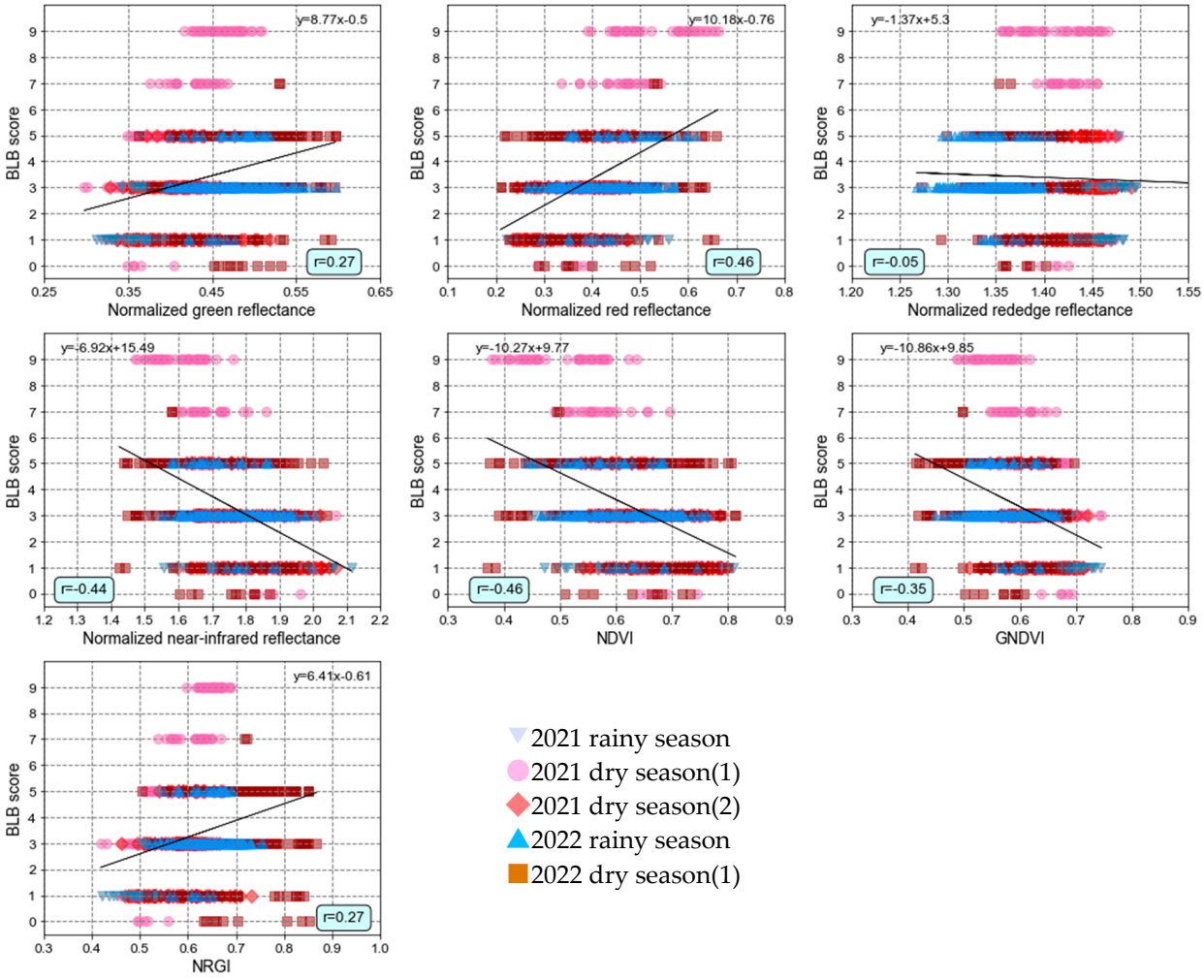

Figure 7. Relationship between UAV data and BLB scores acquired during the 2021 and 2022 dry and rainy seasons.

Table 4. Correlation coefficient between UAV data and BLB score acquired during the 2021 and 2022 dry and rainy seasons (** significant at 1% the level).

	Ngreen	Nred	Nred Edge	NNIR	NDVI	GNDVI	NRGI
Correlation coefficient	0.271 **	0.458 **	−0.049	−0.440 **	−0.456 **	−0.349 **	0.265 **

Next, a correlation analysis was performed between the UAV data and the field damage intensity determined from the BLB scores for all cropping seasons (Figure 8, Table 5). The correlation coefficients for Nred, NNIR, and NDVI exceeded 0.5, which was higher than those of the other normalized reflectance and indices. Similar to the BLB score analysis results, for plots with high correlation coefficients with Nred, NNIR, and NDVI and with more than 70% damage, the amount of data entered with scores 7 and 9 was lower than for other scores, indicating that they may have been difficult to estimate with high accuracy.

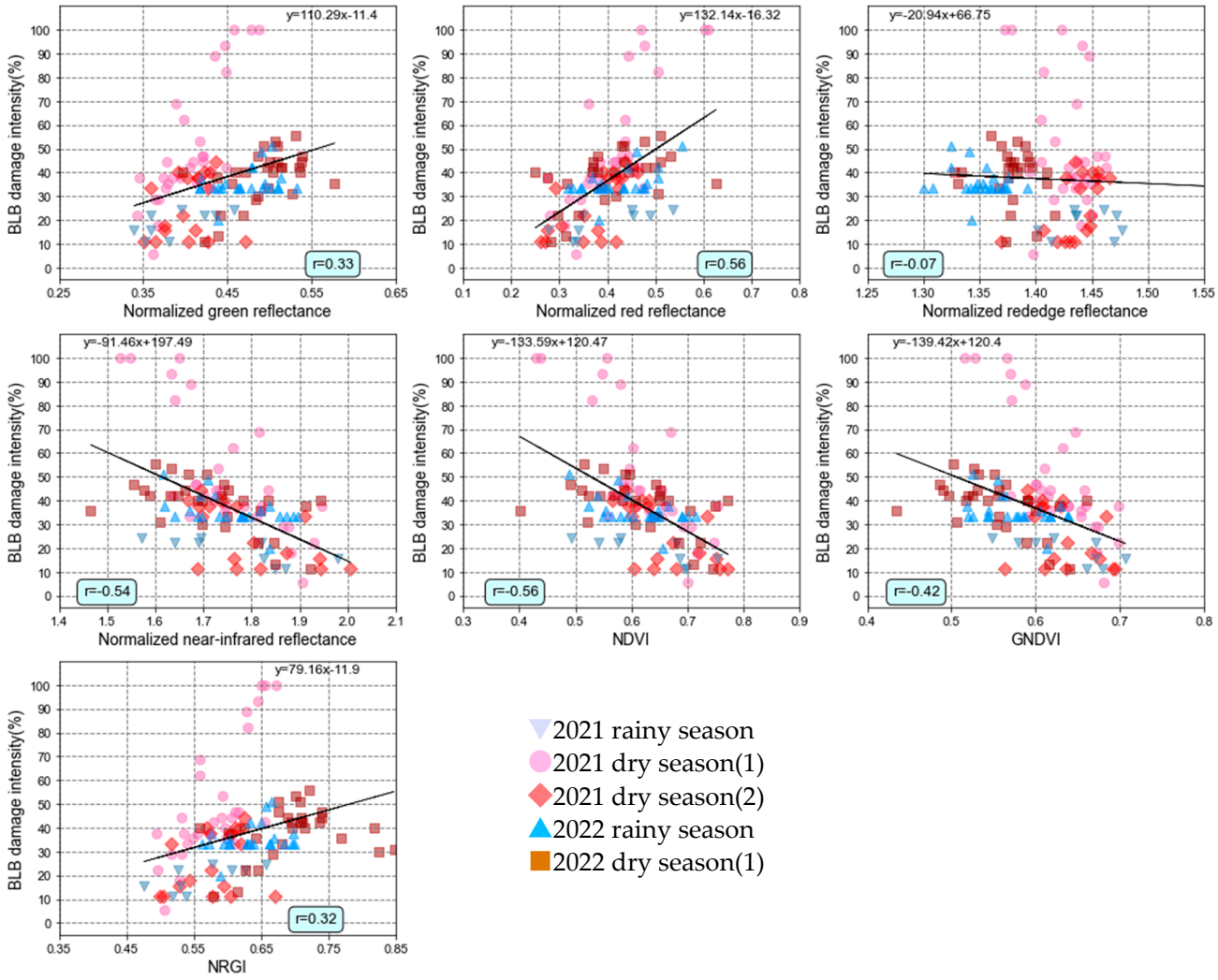

Figure 8. Relationship between UAV data and BLB damage intensity acquired during the 2021 and 2022 dry and rainy seasons.

Table 5. Correlation coefficient between UAV data and BLB damage intensity acquired during the 2021 and 2022 dry and rainy seasons (** significant at the 1% level).

	Ngreen	Nred	Nred Edge	NNIR	NDVI	GNDVI	NRGI
Correlation coefficient	0.329 **	0.558 **	−0.074	−0.537 **	−0.556 **	−0.425 **	0.316 **

As described above, the correlation analysis between the BLB scores and BLB damage intensities revealed normalized reflectance values and indices that may be effective indicators for BLB damage assessment. However, it was suggested that the strength of the correlations differed among the data groups used and that bias in the number of data obtained for each BLB score may have affected the evaluation results. Therefore, we calculated the mean values of the normalized reflectance and index for each BLB score for the 1090 survey points and performed a correlation analysis using the six mean scores (Figure 9, Table 6). For all crop season data, a strong relationship was confirmed for Nred, NNIR, and NDVI, as well as for the relationships among pre-average scores, damage intensities, and UAV data, with correlation coefficients exceeding 0.9. Based on the results of the analysis using the average score, Nred, NNIR, and NDVI had a strong correlation with the BLB score, increasing their possibility of being effective indicators for BLB damage assessment.

In addition, from the viewpoint that the current method is conducted according to visual assessment by the assessors, Nred in the visible range is shown to be an effective index for the estimation formula of the BLB damage assessment.

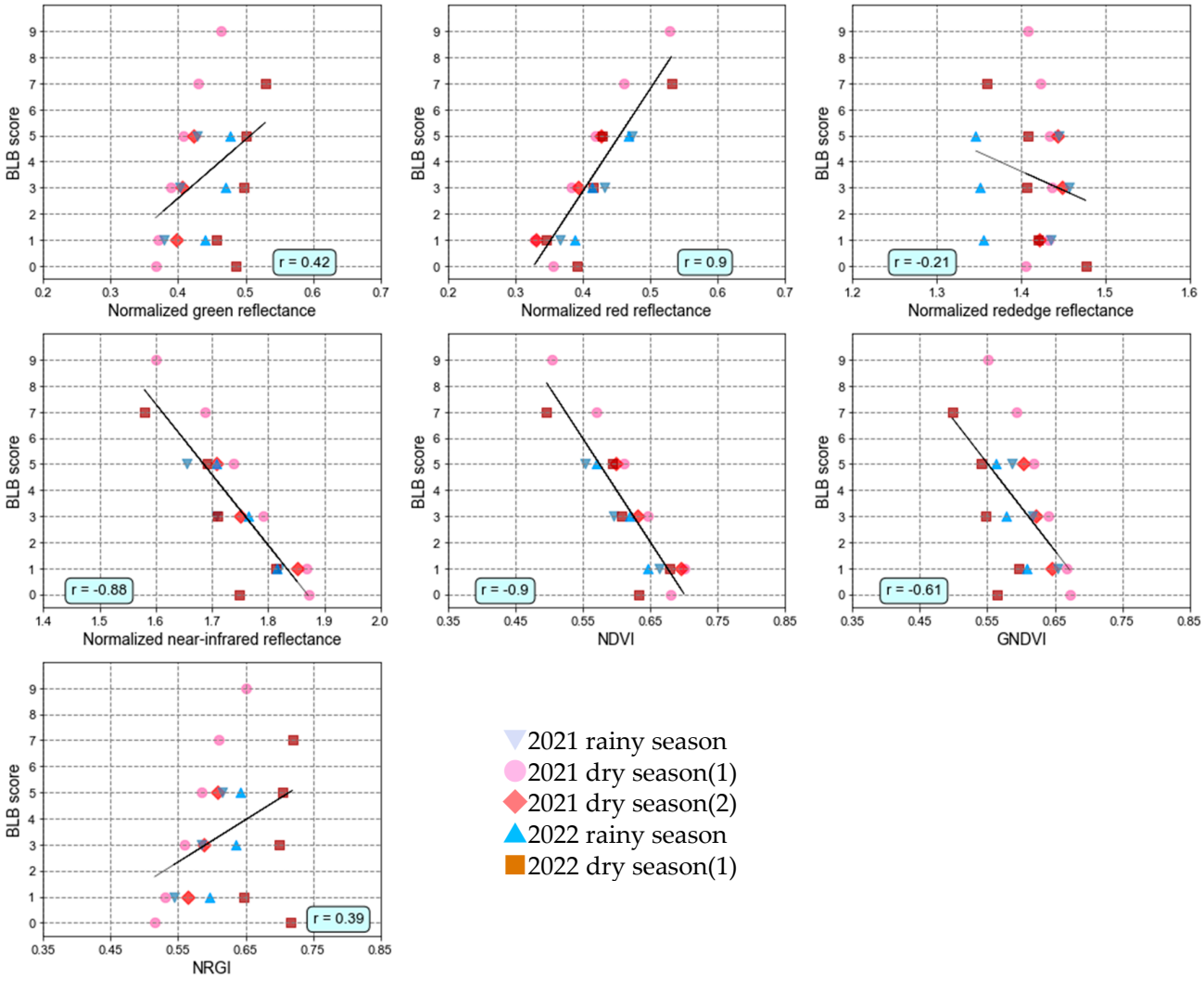

Figure 9. Relationship between UAV data and BLB mean score acquired during the 2021 and 2022 dry and rainy seasons.

Table 6. Correlation coefficient between UAV data and BLB mean score acquired during the 2021 and 2022 dry and rainy seasons (** significant at the 1% level).

	Ngreen	Nred	Nred Edge	NNIR	NDVI	GNDVI	NRGI
Correlation coefficient	0.418 **	0.895 **	−0.211	−0.876 **	−0.897 **	−0.605 **	0.389 **

Nred is the absorption band of chlorophyll; the higher the damage, the lower the chlorophyll content and the higher the reflectance, which may confirm a positive correlation [45–47]. In the case of BLB disease, the leaves fade, with yellowing at the leaf margins and a grayish white color in the case of advanced infection. A negative correlation between SPAD values obtained using a chlorophyll meter and BLB damage intensity [34], and the ability to classify paddy rice with high BLB severity based on the normalized green–red difference index obtained from the RGB base [48], have also been reported in research

covering the same area as this study. Research using hyperspectral data has reported that BLB-infected rice plants show peculiar changes between 757 nm and 1039 nm, corresponding to the near-infrared region, and that reflectance decreases with increasing severity [49]; the same trend was confirmed in this study. The NDVI is the vegetation index calculated from red and near-infrared, and the GNDVI is the vegetation index calculated from green and near-infrared. In this study, we found that Ngreen increased, Nred increased, and NNIR decreased with increasing BLB damage. These results confirmed a negative correlation, because the numerators of the NDVI and GNDVI were smaller when the damage to the BLB was larger. When rice is infected with BLB, the chlorophyll in the leaves decomposes, which leads to a loss of vitality in the rice plant, resulting in changes in the green color of the leaves. This could explain the positive correlation between the Nred band and degree of BLB infection. It is well known that the reflectance of the NIR band and vegetation index are related to the biomass volume and amount of crop production [50].

3.2. BLB Damage Assessment Estimation Equations

As described in Section 3.1, the correlation coefficients between UAV multispectral data categorized according to cropping season and average normalized reflectance in relation to BLB score were the highest for normalized red reflectance and NDVI. This corresponds to the selection of the red band, which is the absorption band of chlorophyll, because the current method allows the assessor to visually assess the degree of BLB damage based on the leaf color. It can also be reasoned that the NDVI, which is related to biomass, was selected because, as the degree of BLB damage progresses, the leaves wither and the crop body becomes smaller than the healthy plant. Therefore, to improve the efficiency of the current method using UAV data, we propose a formula to estimate the BLB score from the normalized red band as an evaluation method, reading the evaluator's decision as a visual one; that is, we used information in the visible range for damage assessment. The equation presented below has a coefficient of determination of 0.92 and RMSE of 1.46 ± 0.36:

$$\text{BLB score} = 50.841 \times \text{NRed(all season)} - 17.475 \quad (7)$$

For validation of the above equation, we used UAV data acquired in 2023, which were not used to create the equation. BLB scores were estimated from normalized red band values calculated from the 2023 UAV data. The estimated BLB score values and the BLB scores assessed by the pest observers were used to calculate the mean absolute percentage error (MAPE) [51], expressed with the following equation:

$$\text{MAPE} = \frac{1}{n}\sum\left|\frac{\text{Gt} - \text{P}}{\text{Gt}}\right| \quad (8)$$

MAPE is given by the average of the absolute value of the ratio of the difference between the ground truth data (Gt) and the estimation (P) to the ground truth, where n represents the number of the data. The MAPE of the BLB score estimated from the data of 70 survey points obtained in February and July 2023 was 9.1%, confirming that the Formula (2) for BLB damage assessment presented in this study was sufficient to be applicable in other years.

A visualization map of the damage assessment using the BLB score estimation equation is shown in Figure 10.

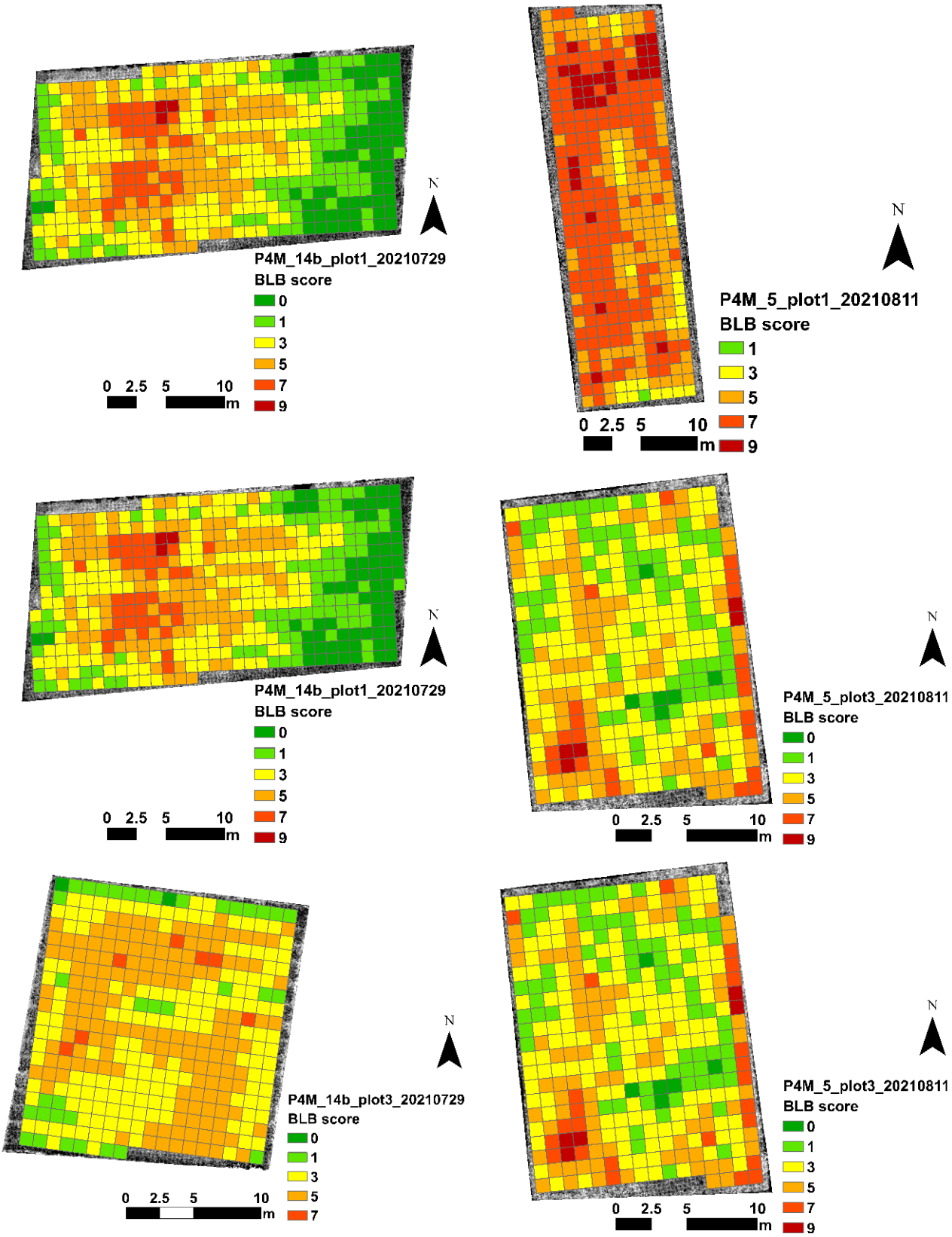

Figure 10. BLB damage assessment score map for dry season in 2021: (**Left**) Block 14b, Plots 1, 2, and 3 from top to bottom; (**Right**) Block 5, Plots 1, 2, and 3 from top to bottom.

3.3. Improvement of Efficiency and Objectivity of BLB Assessment

The effectiveness of using UAV data was examined through applying the constructed formula to estimate the BLB damage during the harvest season, using the red band as an indicator for each irrigated block.

The total time required for the BLB evaluation using UAV data was defined as the sum of the times required for the following processes: acquisition of field survey data and UAV data, uploading and downloading of acquired data, confirmation of acquired data content, preprocessing of UAV data, application of the estimation formula, and creation of evaluation maps. In addition, the assessors conducted a maximum of 12 field-based damage assessment surveys per day using the current method. However, because the number of plots that can be surveyed per day decreases depending on weather conditions, it is expected to take more time in rainy weather.

The time required for both methods and the efficiency gains are listed in Table 7. For example, Irrigation Block 1b contained 60 paddy plots. Using the current method, the evaluator would take 5 days to evaluate all the plots. However, if UAV imagery were integrated into the current method, the evaluation would be completed in 2 days and 3 h, with 57.5% time saving. The greater the number of plots, the greater the percentage of efficiency gain, with a maximum time–cost reduction of 76.4%.

Table 7. Comparison of time required to assess all fields using the current method and the integrated method with UAV data.

Irrigation Block Name	No. of Plots	Area (ha)	Time Required to Assess All Plots Using the Current Method	Time Required to Assess All Plots Using the Integrated Method with UAV Data	Percentage of Time Saved (%)
Block 1b	60	3.1	5 days	2 days and 3 h	57.5
Block 2a	43	2.2	4 days	2 days and 3 h	46.9
Block 3a	62	2.9	6 days	2 days and 3 h	64.6
Block 5	38	2.6	4 days	2 days and 2.5 h	47.4
Blcok 7a	54	2.7	5 days	2 days and 2.5 h	57.5
Block 9b	56	3.4	5 days	2 days and 3 h	57.5
Block 11a	67	2.6	6 days	2 days and 3 h	64.6
Block 11b	104	2.8	9 days	2 days and 3 h	76.4
Block 12a	68	2.9	6 days	2 days and 3 h	64.6
Block 14a	84	2.9	7 days	2 days and 3 h	69.6

An example of an evaluation map visualizing the damage to all paddy fields in an irrigated area obtained via inputting the BLB evaluation estimation equation into a normalized red-band image is shown in Figures 11–13. The numbers at the tops of the bars indicate the number of paddy plots with each damage intensity, and the numbers next to the stars indicate the damage intensities calculated from the three plots using the proposed method. The damage intensities for irrigation Blocks 1b, 9b, and 11b using the proposed method were 33.3%, 33.7%, and 40.7%, respectively. However, the damage intensities estimated from the UAV data differed from plot to plot, and incorporating the UAV data into the current method enabled an objective and complete enumeration.

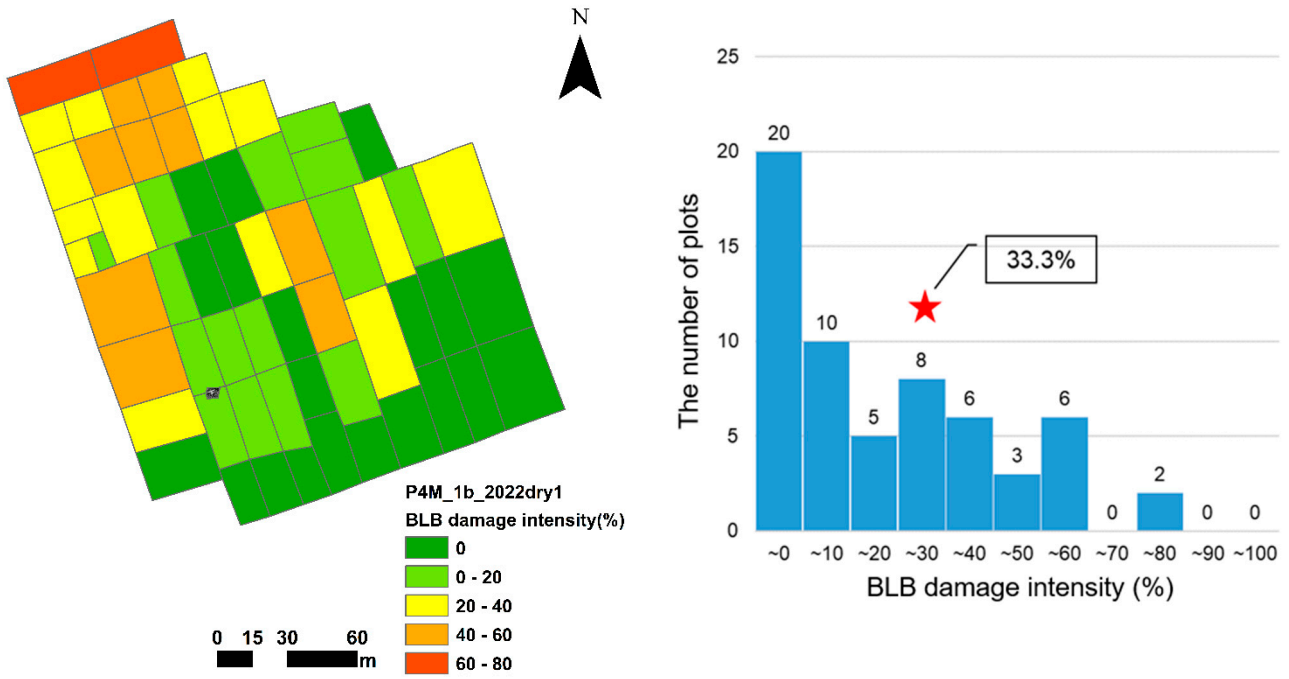

Figure 11. BLB damage assessment intensity map for the dry season in 2022: (**Left**) visualization map of Block 1b; (**Right**) number of paddy plots per damage intensity. (★) BLB damage intensity calculated from three plots using the current damage assessment method described in Section 2.3.

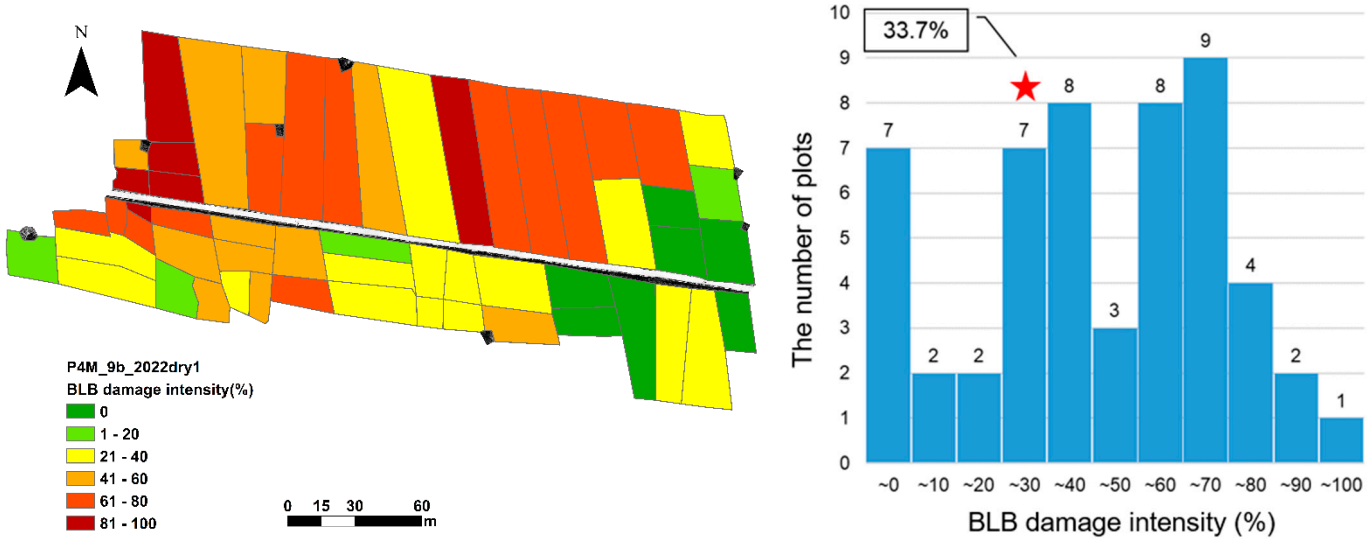

Figure 12. BLB damage assessment intensity map for the dry season in 2022: (**Left**) visualization map of Block 11b; (**Right**) number of paddy plots per damage intensity. (★) BLB damage intensity calculated from three plots using the current damage assessment method described in Section 2.3.

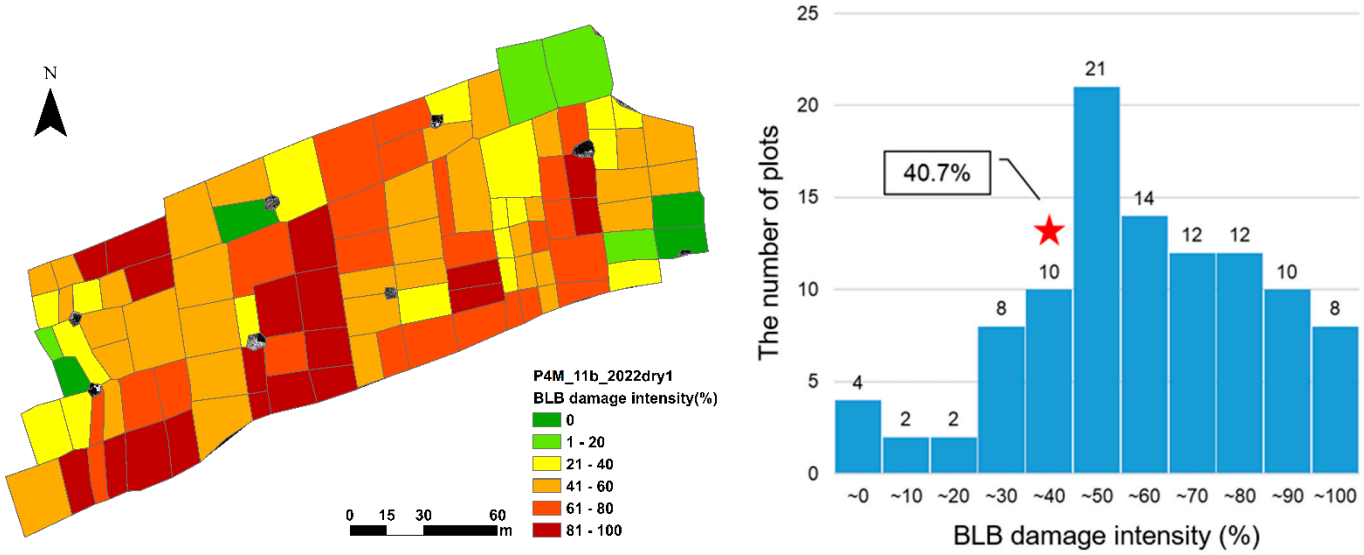

Figure 13. BLB damage assessment intensity map for the dry season in 2022: (**Left**) visualization map of Block 9b; (**Right**) number of paddy plots per damage intensity. (★) BLB damage intensity calculated from three plots using the current damage assessment method described in Section 2.3.

4. Conclusions

Agricultural insurance, which is expected to be a climate change adaptation measure, has been operating as an important social infrastructure for food security. However, there were many challenges in Indonesia soon after its operation. The biggest challenges were speeding up loss assessment, which is the core of agricultural insurance, and the objectivity of the assessment results. In this study, a rapid and objective damage assessment method was developed and implemented in West Java for BLB of rice, a disease covered by insurance.

Based on the analysis of the relationship between the BLB scores, damage intensities, and UAV data acquired during the dry and rainy seasons of 2021 and 2022, a BLB damage assessment estimation equation using normalized red bands was developed. Validation of the equation was performed using the MAPE. The MAPE of the BLB score estimated from the data of 70 survey points obtained in February and July 2023 was 9.1%, confirming that the formula (2) for BLB damage assessment presented in this study was suitable for application to other years' data. We integrated the process of UAV aerial photography and the estimation formula based on UAV data into the current damage assessment steps proposed by the Ministry of Agriculture of Indonesia and implemented in society. The evaluation time was reduced by more than 60% on average, and technical guideline is issued for a new damage evaluation process for agricultural insurance that reduces labor and ensures objectivity.

The national government is in charge of maintaining and improving the agricultural insurance system, while the state government is in charge of practices related to losses. It is necessary to obtain recognition and approval from the Crop Protection Bureau of the Ministry of Agriculture for the evaluation methodology. Therefore, we approached the central ministry regarding the actual operation of the new evaluation method and sent a letter from the Director of the Crop Protection Department of the Ministry of Agriculture supporting the use of the method established in the project to the Director of the West Java Provincial Department of Agricultural Policy, which was highly appreciated by the government. Currently, we aim to accumulate damage assessment data and improve the assessment method through incorporating machine learning and other methods.

Author Contributions: Conceptualization, methodology, and writing—original draft preparation, C.H. and S.I.; investigation, resources, and data curation, G.S., C.H. and S.I.; review and editing, E.T.; funding acquisition, C.H. and E.T.; supervision and project administration, C.H. All authors have read and agreed to the published version of the manuscript.

Funding: This research was funded by Japan Science and Technology Agency (JST) and Japan International Cooperation Agency (JICA), grant Number JPMJSA1604, and JSPS KAKENHI, grant number JP22KK0089.

Data Availability Statement: All data supporting the findings of this study are included in the text.

Acknowledgments: The authors gratefully acknowledge Danan Hidayat, Ir Kustiaman, Yogi Tojiri Septiadi, Hasam Supriatna, Gagan Gandana Wibawa, Adam Daniel, Denny Magria, and Taufik Rahmat from the Provincial Office of Food Crops and Horticulture of West Java Province, Indonesia for contribution to this research and field investigation at the study site.

Conflicts of Interest: Author Shun Isono was employed by the NHK (Japan Broadcasting Corporation). All authors declare that the research was conducted in the absence of any commercial or financial relationships that could be construed as a potential conflict of interest.

References

1. IPCC-Sixth Assessment Report. Available online: https://www.ipcc.ch/assessment-report/ar6/ (accessed on 23 February 2024).
2. Gurdeep, S.M.; Manpreet, K.; Prashant, K. Impact of Climate Change on Agriculture and Its Mitigation Strategies. *Sustainability* **2021**, *13*, 1318. [CrossRef]
3. Sameh, K.A.; Miriam, M.; Antonio, J.; Mariá, A.; Jonathan, D.P.; Laurence, J.; Zhenhua, Z.; Paulo, P.; Luuk, F.; Martine, P.; et al. Climate change impacts on agricultural suitability and yield reduction in a Mediterranean region. *Geoderma* **2020**, *374*, 114453. [CrossRef]
4. Muhammad, H.; Ashfaq, A.; Ahsan, R.; Muhammad, U.H.; Hesham, F.A.; Yahya, M.A.; Atif, A.B.; Khalid, R.H.; Saeed, A.; Wajid, N.; et al. Impact of climate change on agricultural production; Issues, challenges, and opportunities in Asia. *Plant Sci.* **2022**, *13*, 925548. [CrossRef] [PubMed]
5. FAOSAT, Food and Agriculture Organization of the United Nations. 2018. Available online: https://www.fao.org/faostat/en/#data/QC (accessed on 23 February 2024).
6. Muhammad, Y.Y.; Rahmat, F.; Teuku, S.B.; Hafizh, M.; Juli, F. Design of Islamic Agricultural Insurance Model: Evidence from Indonesia. *Int. J. Sustain. Dev. Plan.* **2022**, *17*, 2375–2384. [CrossRef]
7. Sahat, M.P. Developing rice farm insurance in Indonesia. *Agric. Agric. Sci. Procedia* **2010**, *1*, 33–41. [CrossRef]
8. Nyoman, Y.; Luh, P.K.P.; Made, B. Effectiveness of Agricultural Insurance Program as A Sustainable Agricultural Development Effort. *Sustain. Environ. Agric. Sci.* **2022**, *6*, 134–143. [CrossRef]
9. Abdul, H.; Rusli, R.; Dan, U.N. The Relationship between the Knowledge Level of Farmers and the Effectiveness of the Rice-Farming Business Insurance Program (AUTP) in Pinrang Regency, South Sulawesi, Indonesia. *Int. J. Soc. Sci. Educ. Res. Stud.* **2022**, *2*, 298–307.
10. Sahat, M.P. *Implementation of Indemnity-Based Rice Crop Insurance in Indonesia*; Food and Fertilizer Technology Center for the Asian and Pacific Region: Taipei, Taiwan, 2016; Available online: https://ap.fftc.org.tw/article/1079 (accessed on 10 March 2024).
11. Adhitya, M.; Sahara, A.D. Analysis of Implementation of Rice Farming Insurance: Case Study In Indonesia. *Dev. Ctry. Stud.* **2016**, *6*, 13–118.
12. Chinna, G.S.; Hari, K.K.; Valli, K.V.; Alakananda, M.; Preethi, A. Deep learning for rice leaf disease detection: A systematic literature review.on emerging trends, methodologies and techniques. *Inf. Process. Agric.* 2024, *in press*. [CrossRef]
13. Lin, S.; Yao, Y.; Li, J.; Li, X.; Ma, J.; Weng, H.; Cheng, Z.; Ye, D. Application of UAV-Based Imaging and Deep Learning in Assessment of Rice Blast Resistance. *Rice Sci.* **2023**, *30*, 652–660. [CrossRef]
14. Sourav, K.B.; Krishna, P.K.; Rajermani, T. A Machine Intelligent Framework for Detection of Rice Leaf Diseases in Field Using IoT Based Unmanned Aerial Vehicle System. *Sparkling Light Trans. Artif. Intell. Quantum Comput. (STAIQC)* **2022**, *2*, 42–51.
15. Shaodan, L.; Jiayi, L.; Deyao, H.; Zuxin, C.; Lirong, X.; Dapeng, Y.; Haiyong, W. Early Detection of Rice Blast Using a Semi-Supervised Contrastive Unpaired Translation Iterative Network Based on UAV Images. *Plants* **2023**, *12*, 3675. [CrossRef] [PubMed]
16. Hongo, C.; Tsuzawa, T.; Tokui, K.; Tamura, E. Development of Damage Assessment Method of Rice Crop for Agricultural Insurance Using Satellite Data. *J. Agric. Sci.* **2015**, *7*, 59–71. [CrossRef]
17. Hongo, C.; Gunardi, S.; Shikata, R.; Niwa, K.; Tamura, E. The Use of Remotely Sensed Data for Estimating of Rice Yield Considering Soil Characteristics. *J. Agric. Sci.* **2014**, *6*, 172–184. [CrossRef]
18. Sofue, Y.; Hongo, C.; Manago, N.; Gunardi, S.; Homma, K.; Baba, B. Estimation of Normal Rice Yield Considering Heading Stage Based on Observation Data and Satellite Imagery. In Proceedings of the 2021 IEEE International Geoscience and Remote Sensing Symposium IGARSS, Brussels, Belgium, 11–16 July 2021; pp. 6439–6442. [CrossRef]

19. Manago, N.; Hongo, C.; Sofue, Y.; Gunardi, S.; Budi, U. Transplanting date estimation using Sentinel-1 satellite data for paddy rice damage assessment in Indonesia. *Agriculture* **2020**, *10*, 625. [CrossRef]
20. Iwahashi, Y.; Gunardi, S.; Budi, U.; Iskandar, L.; Ahmad, J.; Bambang, H.T.; IMade, A.S.W.; Maki, M.; Hongo, C.; Homma, K. Drought Damage Assessment for Crop Insurance Based on Vegetation Index by Unmanned Aerial Vehicle Multispectral Images of Paddy Fields in Indonesia. *Agriculture* **2023**, *13*, 113. [CrossRef]
21. Inoue, T. Satellite- and drone-based remote sensing of crops and soils for smart farming—A review. *Soil Sci. Plant Nutr.* **2020**, *66*, 798–810. [CrossRef]
22. Inoue, Y. Remote Sensing of Plant and Soil Information by High-resolution Op-tical Satellite Sensors and Its Applications to Smart Agriculture. *J. Remote Sens. Soc. Jpn.* **2017**, *37*, 213–223.
23. Jean, R.F.M.; Yamashita, M.; Yoshimura, M.; Enrico, C.P. Leaf Spectral Analysis for Detection and Differentiation of Three Major Rice Diseases in the Philippines. *Remote Sens.* **2023**, *15*, 3058. [CrossRef]
24. Singh, B.; Singh, M.; Singh, G.; Suri, K.; Pannu, P.P.S.; Bal, S.K. Hyper-Spectral Data for The Detection of Rice Bacterial Leaf Blight (BLB) Disease. *Proc. AIPA* **2012**, *2012*, 177–182.
25. Wijaya, I.M.A.S.; Chandra, I.G.B.E.; Hongo, C. Assessment of bacterial leaf blight (BLB) diseases by unmanned aerial vehicle (UAV)-based vegetation index of paddy fields. In Proceedings of the 10th Asian-Australasian Conference on Precision Agriculture (ACPA10), Universiti Putra Malaysia, Seri Kembangan, Malaysia, 24–26 October 2023.
26. Yuti, G.; Hongo, C.; Saito, D.; Caasi, O.; Susilawati, P.N.; Shishido, M.; Sudiarta, I.P.; Wijaya, I.M.A.S.; Homma, K. Evaluating Multispectral Imaging for Assessing Bacterial Leaf Blight Damage in Indonesian Agricultural Insurance. In *E3S Web of Conferences*; EDP Sciences: Les Ulis, France, 2021; Volume 232.
27. Kobayashi, T.; Sasahara, M.; Kanda, E.; Ishiguro, K.; Hase, S.; Torigoe, Y. Assessment of Rice Panicle Blast Disease Using Airborne Hyperspectral Imagery. *Open Agric. J.* **2016**, *10*, 28–34. [CrossRef]
28. Zhao, D.; Cao, Y.; Li, J.; Cao, Q.; Li, J.; Guo, F.; Feng, S.; Xu, T. Early Detection of Rice Leaf Blast Disease Using Unmanned Aerial Vehicle Remote Sensing: A Novel Approach Integrating a New Spectral Vegetation Index and Machine Learning. *Agronomy* **2024**, *14*, 602. [CrossRef]
29. Yamaguchi, T.; Tanaka, Y.; Imachi, Y.; Yamashita, M.; Katsura, K. Feasibility of Combining Deep Learning and RGB Images Obtained by Unmanned Aerial Vehicle for Leaf Area Index Estimation in Rice. *Remote Sens.* **2021**, *13*, 84. [CrossRef]
30. Ning, L.; Jie, Z.; Zixu, H.; Dong, L.; Qiang, C.; Xia, Y.; Yongchao, T.; Yan, Z.; Weixing, C.; Tao, C. Improved estimation of aboveground biomass in wheat from RGB imagery and point cloud data acquired with a low-cost unmanned aerial vehicle system. *Plant Methods* **2019**, *15*, 17. [CrossRef] [PubMed]
31. Shi, Y.; Huang, W.; Ye, H.; Ruan, C.; Xing, N.; Geng, Y.; Dong, Y.; Peng, D. Partial Least Square Discriminant Analysis Based on Normalized Two-Stage Vegetation Indices for Mapping Damage from Rice Diseases Using PlanetScope Datasets. *Sensors* **2018**, *18*, 1901. [CrossRef]
32. Zheng, Q.; Huang, W.; Cui, X.; Shi, Y.; Liu, L. New Spectral Index for Detecting Wheat Yellow Rust Using Sentinel-2 Multispectral Imagery. *Sensors* **2018**, *18*, 868. [CrossRef] [PubMed]
33. Prabir, K.D.; Laxman, B.; Kameswara, S.V.C.R.; Seshasai, M.V.R.; Dadhwal, V.K. Monitoring of bacterial leaf blight in rice using ground-based hyperspectral and LISS IV satellite data in Kurnool, Andhra Pradesh, India. *Int. J. Pest Manag.* **2015**, *61*, 359–368. [CrossRef]
34. Caasi, O.; Hongo, C.; Suryaningsih, A.; Wiyono, S.; Homma, K.; Shishido, M. Relationships between bacterial leaf blight and other diseases based on field assessment in Indonesia. *Trop. Agric. Dev.* **2019**, *63*, 113–121. [CrossRef]
35. Caasi, O.; Hongo, C.; Wiyono, S.; Giamerti, Y.; Saito, D.; Homma, K.; Shishido, M. The potential of using sentinel-2 satellite imagery in assessing bacterial leaf blight on rice in West Java, Indonesia. *J. Int. Soc. Southeast Asia Agric. Sci.* **2020**, *26*, 1–16.
36. Hongo, C.; Takahashi, Y.; Gunardi, S.; Budi, U.; Tamura, E. Advanced Damage Assessment Method for Bacterial Leaf Blight Disease in Rice by Integrating Remote Sensing Data for Agricultural Insurance. *J. Agric. Sci.* **2022**, *14*, 1–18. [CrossRef]
37. Syed, A.H.N.; Rashida, P.; Ummad, D.U.; Owais, M.; Ateequr, R.; Sajid, W.; Taha, M. Determination of antibacterial activity of various broad spectrum antibiotics against Xanthomonas oryzae pv. Oryzae, a cause of bacterial leaf blight of rice. *Int. J. Microbiol. Mycol.* **2014**, *2*, 12–19.
38. Bai, X.; Zhou, Y.; Feng, X.; Tao, M.; Zhang, J.; Deng, S.; Lou, B.; Yang, G.; Wu, Q.; Yu, L.; et al. Evaluation of rice bacterial blight severity from lab to field with hyperspectral imaging technique. *Plant Sci.* **2022**, *13*, 1037774. [CrossRef]
39. Chukwu, S.C.; Rafii, M.Y.; Ramlee, S.I.; Ismail, S.I.; Hasan, M.M.; Oladosu, Y.A.; Magaji, U.G.; Akos, I.; Olalekan, K.K. Bacterial leaf blight resistance in rice: A review of conventional breeding to molecular approach. *Mol. Biol. Rep.* **2019**, *46*, 1519–1532. [CrossRef]
40. Mohammad, M.F.A.; Han, Y.L. Advanced diagnostic approaches developed for the global menace of rice diseases. *Can. J. Plant Pathol.* **2022**, *44*, 627–651. [CrossRef]
41. Hashimoto, N.; Saito, Y.; Maki, M.; Homma, K. Simulation of reflectance and vegetation indices for unmanned aerial vehicle (UAV) monitoring of paddy fields. *Remote Sens.* **2019**, *11*, 2119. [CrossRef]
42. Rice Knowledge Bank, IRRI. Available online: http://www.knowledgebank.irri.org/decision-tools/rice-doctor/rice-doctor-fact-sheets/item/bacterial-blight (accessed on 17 May 2024).
43. Tabasia, A.; Vishal, G.; Aarushi, S.; Sheikh, S.K. Effect of Weather Parameters on the Severity of Bacterial Leaf Blight of Rice. *Biol. Forum Int. J.* **2022**, *14*, 123–133.

44. Krishnan, N.; Gandhi, K.; Mohammed, F.P.; Muthuraj, R.; Kuppusamy, P.; Thiruvengadam, R. Management of Bacterial Leaf Blight Disease in Rice with Endophytic Bacteria. *World Appl. Sci. J.* **2013**, *28*, 2229–2241.
45. Qiao, L.; Tang, W.; Gao, D.; Zhao, R.; An, L.; Li, M.; Sun, H.; Song, D. UAV-based chlorophyll content estimation by evaluating vegetation index responses under different crop coverages. *Comput. Electron. Agric.* **2022**, *196*, 106775. [CrossRef]
46. Gu, Q.; Huang, F.; Lou, W.; Zhu, Y.; Hu, H.; Zhao, Y.; Zhou, H.; Zhang, X. Unmanned aerial vehicle-based assessment of rice leaf chlorophyll content dynamics across genotypes. *Comput. Electron. Agric.* **2024**, *221*, 108939. [CrossRef]
47. Nikolas, P.; Dionissios, K.; Rigas, G. Spatial Analysis of Agronomic Data and UAV Imagery for Rice Yield Estimation. *Agriculture* **2021**, *11*, 809. [CrossRef]
48. Nor, H.A.; Rohayu, H.N.; Tajul, R.R.; Siti, A.A.; Noorfatekah, T.; Zulkiflee, A.L.; Norhashila, H.; Khairulazhar, Z. Detection of Bacterial Leaf Blight Disease Using RGB-Based Vegetation Indices and Fuzzy Logic. In Proceedings of the 2023 19th IEEE International Colloquium on Signal Processing & Its Applications, Kedah, Malaysia, 3–4 March 2023. [CrossRef]
49. Chwen, M.Y. Assessment of the severity of bacterial leaf blight in rice using canopy hyperspectral reflectance. *Precis. Agric.* **2010**, *11*, 61–81. [CrossRef]
50. Taifeng, D.; Jiangui, L.; Budong, Q.; Liming, H.; Jane, L.; Rong, W.; Qi, J.; Catherine, C.; Heather, M.; Jarrett, P.; et al. Estimating crop biomass using leaf area index derived from Landsat 8 and Sentinel-2 data. *J. Photogramm. Remote Sens.* **2020**, *168*, 236–250. [CrossRef]
51. Brenon, D.S.B.; Gabriel, A.S.F.; Lucas, C.; Yiannis, A.V.V.; Luana, M.S. UAV-based coffee yield prediction utilizing feature selection and deep learning. *Smart Agric. Technol.* **2021**, *1*, 100010. [CrossRef]